ACS APPLIED BIO MATERIALS

www.acsabm.org Article

Photocurable Albumin Methacryloyl Hydrogels as a Versatile Platform for Tissue Engineering

Gaia Ferracci, Mengxiang Zhu, Mohammed Shahrudin Ibrahim, Gamaliel Ma, Teng Fei Fan, Bae Hoon Lee,* and Nam-Joon Cho*

Cite This: *ACS Appl. Bio Mater.* 2020, 3, 920−934 Read Online

ACCESS | Metrics & More | Article Recommendations | Supporting Information

ABSTRACT: Photopolymerization of protein-derived polymers functionalized with methacryloyl groups has been increasingly used to fabricate three-dimensional tissue constructs for biomedical applications because photocurable protein-based polymers (e.g., gelatin and collagen methacryloyl) feature spatial-temporal controllability of engineering complex constructs as well as inherent biological properties. Herein, we report photocurable albumin-based hydrogels. First, photocurable bovine serum albumin methacryloyl (BSA-MA) with different degrees of substitution (DM) was successfully synthesized in a precise manner, without substantially altering BSA native secondary structure. Resultant photocurable BSA-MA hydrogels exhibited tunable physio-biochemical properties over the swelling, degradation, and mechanical properties. Moreover, photo-cross-linked BSA-MA hydrogels provided a permissible environment to support cell viability and functionality both in two- and three-dimensional culture systems. Photocurable BSA-MA hydrogels may be used as a versatile platform for various bioapplications including tissue engineering and 3D bioprinting.

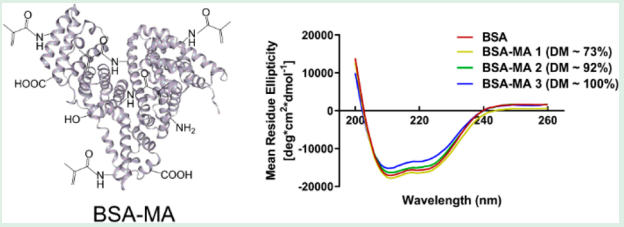

KEYWORDS: *bovine serum albumin, bovine serum albumin methacryloyl, photocurable hydrogels, tunable properties, tissue engineering, three-dimensional scaffolds*

INTRODUCTION

Hydrogels, due to their high water content and a broad range of physicochemical properties, have been increasingly explored for tissue engineering applications.[1−3] Both synthetic and natural polymers have been utilized to fabricate biocompatible water-swollen polymer networks that mimic the in vivo microenvironment.[4,5] Synthetic polymer-based hydrogels can be reproducibly manufactured on a large scale at low cost and possess mechanical properties that can be easily controlled but lack cell-recognition sites, even though these can be provided through the incorporation of biological molecules. Natural polymer-based hydrogels, instead, bear specific cell interaction sites crucial for biocompatibility and biodegradability but usually possess poor mechanical properties even though these can be improved through chemical cross-linking strategies.[6,7] The formation of intermolecular covalent bonds between the polymer chains can be achieved by means of radical photopolymerization or addition/condensation polymerization; however, photoinitiated radical polymerization has been preferentially used to fabricate hydrogels for biomedical applications due to the spatial-temporal precision of the cross-linking process, the possibility of manufacturing complex structures in a fast and facile manner, and the easily tunable properties of the resulting hydrogels.[7] Functional polymers have been fabricated with photocurable moieties (e.g., acryloyl or methacryloyl groups) upon ultraviolet (UV) or visible light in the presence of a photoinitiator creating covalent bonds, resulting in a cross-linked polymer network.[7,8] Methacryloylation of natural polymers such as collagen,[9] gelatin,[10−13] hyaluronic acid,[13,14] chitosan,[15] alginate,[16] dextran,[17,18] chondroitin sulfate,[13] silk,[19] and tropoelastin[20] has been reported as a promising strategy to fabricate hydrogel constructs for a variety of biomedical applications.

Albumin is one of the most abundant proteins in blood plasma (35−50 mg mL^{-1} in humans), plays a crucial role in regulating the plasma oncotic pressure, acts as a carrier of metal ions and various endogenous and exogenous molecules, and possesses antioxidant properties.[21,22] In addition, albumin primary sequence and heart shape folded tertiary structure are well-known, facilitating the design of albumin-based applications such as scaffolds for cell culture or systems for drug delivery.[22−25] For instance, by knowing the exact 3D arrangement of various amino acids, simulations to determine the interactions between albumin and therapeutic substances can be performed, and prediction of albumin ligand-binding abilities can be achieved,[26] which can be advantageous in the

Received: October 23, 2019
Accepted: December 30, 2019
Published: January 13, 2020

https://dx.doi.org/10.1021/acsabm.9b00984
ACS Appl. Bio Mater. 2020, 3, 920−934

Table 1. Experimental Parameters Used during Synthesis of BSA-MA[a]

samples	synthesis methods	batch (g)	MAA (94%, mL)	mole ratio MAA/lysine	0.25 M CB buffer (mL)	T (°C)	time (h)	initial pH	yield (%)
BSA-MA 1	sequential addition	20	1.558	0.55	200	37	1	9	87
BSA-MA 2	sequential addition	20	3.116	1.1	200	37	1	9	94
BSA-MA 3	sequential addition	20	6.233	2.2	200	37	1	9	93
BSA-MA 4	sequential addition	20	12.465	4.4	200	37	1	9	90

[a]MAA, methacrylic anhydride; CB, carbonate-bicarbonate; T, temperature.

development of drug delivery systems. As a result, human serum albumin (HSA) has been successfully employed as a drug carrier in a few FDA approved medicines for the treatment of diabetes and various types of cancer.[22,23] Furthermore, over the past 15 years, albumin has also been explored for various tissue engineering applications.[24,25] Among these, the ones focusing on the use of bovine serum albumin (BSA) demonstrated the potential of this protein as a scaffold biomaterial for in vivo implants[27] and for in vitro culture of human mesenchymal stem cells,[28] human induced pluripotent stem cells,[29] fibroblasts,[30] muscle cells,[30] endothelial cells,[30] and cardiomyocytes.[31,32]

In these studies, BSA was chosen as a valid alternative to human serum albumin (HSA) due to its vast availability, low cost, and molecular structure similarity to HSA. However, the fabrication of BSA scaffolds mainly relied on the denaturation or unfolding of BSA molecules, which might result in altered protein functionality. Specifically, via the use of low pH solutions[27,31] or reducing agents (e.g., β-mercaptoethanol,[29,30,32] dithiothreitol[28]), which respectively caused intramolecular static charge repulsions and disulfide bonds reduction, BSA molecules passed from a native protein globular structure to an unfolded conformation. In this extended form, BSA molecules were assembled and refolded in a non-native structure, via self-assembly of exposed hydrophobic domains,[27] spontaneous formation of new intra- and intermolecular disulfide bonds,[29,30,32] or formation of new intra- and intermolecular bonds in the presence of cross-linking agents (e.g., microbial transglutaminase[28]), leading to the fabrication of non-native BSA-based scaffolds. However, passing from a native globular conformation to a non-native refolded structure resulted in altered protein binding affinities, with a reduced number of sites available for the binding of all-trans retinoic acid molecules.[27] Moreover, receptors (e.g., albondin, calreticulin, and heterogeneous nuclear ribonucleoproteins) binding albumin in its native conformation have been identified in various types of cells.[21] Therefore, changes in the native BSA heart-shape folded tertiary structure might impact the innate BSA capacity to ligate cell-membrane receptors and chemical compounds. Thus, fabrication of constructs where the native BSA heart-shape conformation is maintained might be advantageous for drug delivery or tissue engineering applications. On the other hand, Iemma et al. reported the fabrication of BSA-based spherical microparticles for oral drug delivery via reverse-phase suspension radical copolymerization of methacrylated BSA and either *N*,*N*-dymethylacrylamide or methacrylic acid sodium salt or *N*-isopropylacrylamide. Methacrylated BSA was obtained by reacting BSA with methacrylic anhydride at controlled pH and temperature, thus to maintain the water solubility and folded structure of native BSA molecules, and the BSA-based microspheres showed pH-dependent swelling behavior and ability to encapsulate and differentially release various types of drugs.[33−36] Abbate et al., instead, fabricated BSA-based hydrogels via photopolymerization of methacrylated BSA and the cross-linking agent *N*,*N*′-methylenebis(acrylamide) and reported that it was not possible to obtain hydrogels in the absence of the cross-linking agent, most probably due to the low degree of functionalization of the synthesized methacrylated BSA.[37] Nonetheless, their BSA-based hydrogels partially retained the esterolytic activity of native BSA, demonstrating potential for protein-based biomimetic catalysts. However, their reports of methacrylated BSA seem preliminary, and until now, photocurable BSA methacryloyl has not been thoroughly scrutinized for tissue engineering applications.

Therefore, the aim of the present study is to systematically investigate photocurable BSA methacryloyl hydrogels as a new platform for tissue engineering applications. BSA methacryloyl samples with different degrees of substitution were successfully prepared via a one-pot method.[38] BSA-MA secondary structure was analyzed, and BSA-MA hydrogel features such as swelling, mechanical properties, and enzymatic degradation were examined in terms of physical tunability. Moreover, cell viability and functionality of BSA-MA hydrogels were also evaluated using a model cell both in two- and three-dimensional culture systems. Our report would spark interest in photocurable BSA-MA hydrogels for potential use in biomedical applications including cell culture, tissue engineering, and 3D bioprinting.

MATERIALS AND METHODS

Synthesis of Bovine Serum Albumin Methacryloyl (BSA-MA). BSA-MA was synthesized similarly according to a method previously utilized for the synthesis of gelatin methacryloyl (gelMA).[39] BSA (V900933; Sigma-Aldrich) was dissolved at 10% w/v into 200 mL of a 0.25 M carbonate-bicarbonate (CB) buffer (14.65 g of sodium bicarbonate and 21.53 g of sodium carbonate decahydrate in 1 L distilled water) under magnetic stirring (500 rpm) at 37 °C. After the complete dissolution of the BSA, the pH of the buffer solution was adjusted to 9 using a 5 M sodium hydroxide solution (NaOH; Sigma-Aldrich). Different amounts of methacrylic anhydride (MAA, 94%; Sigma-Aldrich), corresponding to different molar ratios of MAA to lysine groups as indicated in Table 1, were then sequentially added to the BSA solution. The reaction proceeded for 1 h under magnetic stirring (500 rpm) at 37 °C and was terminated by adjusting the pH of the solution to 7.4 using a 6 M hydrochloric acid solution (HCl; Sigma-Aldrich) or a 5 M NaOH solution. The solution was filtered using sequentially 70 mm filter papers, and then dialyzed against distilled water for 4−6 h at room temperature using a tangential flow filtration (TFF) system equipped with a Pellicon 2 cassette containing a 10 kDa Biomax membrane (Merck Millipore), to remove unreacted MAA and methacrylic acid byproduct. At last, BSA-MA solutions were freeze-dried for 4−5 days and stored at −20 °C until further use.

Degree of Methacryloylation. After the incorporation of methacryloyl groups into BSA, the degree of methacryloylation (DM) of the various BSA-MA samples was quantitatively determined by 2,4,6-trinitrobenzenesulfonic acid (TNBS) assay and qualitatively verified through nuclear magnetic resonance (NMR) spectroscopy.

https://dx.doi.org/10.1021/acsabm.9b00984
ACS Appl. Bio Mater. 2020, 3, 920−934

TNBS assay was performed similarly according to what was previously described.[40] BSA and BSA-MA samples were separately dissolved at 0.2 mg mL^{-1} in a 0.1 M sodium bicarbonate ($NaHCO_3$) buffer (pH 8.5) at room temperature. Then 0.5 mL of a 0.01% w/v TNBS (Sigma-Aldrich) solution (in 0.1 M $NaHCO_3$ buffer) was added to 0.5 mL of each sample solution, and the mixtures were incubated at 37 °C for 2 h. To stop the reaction, 0.5 mL of 10% w/v sodium dodecyl sulfate (SDS; Sigma-Aldrich) and 0.25 mL of 1 M HCl were added, and the absorbance of each solution was measured at 335 nm using a microplate reader (Infinite M200 Pro; Tecan AG). Glycine standard solutions at 16, 8, 4 2, 1, and 0 $\mu g\ mL^{-1}$, prepared by serial dilutions in 0.1 M $NaHCO_3$ buffer, were used to plot a standard curve and determine the molar concentration of free primary amino groups in each sample (Figure S1). The degree of methacryloylation (DM) was calculated according to the following formula

$$\text{DM } \% = \left(1 - \frac{M_{\text{BSA-MA}}}{M_{\text{BSA}}}\right) \times 100$$

where $M_{\text{BSA-MA}}$ and M_{BSA} are the molarity of the free primary amino groups in the BSA-MA and BSA samples, respectively.

For proton nuclear magnetic resonance (^{1}H NMR) spectroscopy, BSA and BSA-MA samples were dissolved at 75 mg mL^{-1} in deuterium oxide (D_2O; Merck) containing 0.1% w/v sodium-3-(trimethylsilyl)propionate (TMSP, D 98%; Cambridge Isotope Laboratories) as a chemical shift reference.[41] ^{1}H NMR spectra were collected at room temperature using an Avance I 400 MHz NMR spectrometer (Bruker). Before analysis, the baseline and the phase of all NMR spectra were corrected, and their chemical shift scale was adjusted to the TMSP signal ($\delta(^1\text{H}) = 0$ ppm).

Secondary Structure of BSA and BSA-MA. The secondary structure of BSA and BSA-MA samples was evaluated using circular dichroism (CD) spectroscopy and attenuated total reflectance-Fourier transform infrared (ATR-FTIR) spectroscopy.

CD spectra of BSA and BSA-MA samples (0.5 mg mL^{-1} in deionized water) were acquired in triplicate with an AVIV model 420 spectrometer (AVIV Biomedical), from 180 to 260 nm at 25 °C, with 1 nm intervals, 1 s averaging time, and 1 nm bandwidth in a 0.1 mm path length quartz cuvette (HellmaAnalytics). Acquired spectra were smoothed (Savitsky-Golay smoothing, third order polynomial, 20 points smoothing window)[42] and normalized by subtracting the spectra of the blank (deionized water). The resulting spectra in millidegrees of ellipticity were converted to mean residue ellipticity (MRE; deg cm^2 $dmol^{-1}$) according to the following formula:[42,43]

$$\text{MRE} = \frac{\theta \times \text{MRW}}{l^{*}c}$$

where θ is the measured resulting ellipticity in mdeg, MRW is the mean residue weight (calculated by dividing the BSA molecular mass in Da by the number of BSA amino acids minus 1[43]), l is the path length in mm, and c is the protein concentration in mg mL^{-1}. The fractional helicity percentage of BSA and BSA-MA samples was calculated based on the MRE value at 208 nm (θ_{208}) according to the following formula:[44]

$$\text{Fractional helicity } \% = \frac{\theta_{208} - \theta_R}{-\theta_\alpha - \theta_R} \times 100$$

where θ_R is the MRE at 208 nm of a protein 100% in a random conformation (−4000 deg cm^2 $dmol^{-1}$), and θ_α is the MRE at 208 nm of a protein 100% α-helix (−33 000 deg cm^2 $dmol^{-1}$).

ATR-FTIR spectra of BSA and BSA-MA samples (30 μL), dissolved in deionized water at 10 mg mL^{-1}, were recorded in triplicate using a Vertex 70 FTIR spectrometer (Bruker) equipped with a mercury cadmium telluride photodetector (Bruker) and a MIRacle ATR accessory module with a three-reflection ZnSe ATR crystal (PIKE Technologies). Spectra were acquired from 4000 to 1000 cm^{-1} using a 4 cm^{-1} resolution and an average of 128 scans. To remove the water and water vapor contribution from the collected spectra, the spectra of the blank aqueous solvent and water vapor were subtracted from those of each sample. The resulting spectra were baseline-corrected and normalized. The spectra in the amide I band region (1700−1600 cm^{-1}) were then deconvoluted using a Gaussian curve fitting to discern the relative contributions of the different secondary structure motifs; the peak centers were determined using a second-derivative analysis and were assigned according to the literature (α-helix 1653−1654 cm^{-1}; β-turn 1675−1680 cm^{-1}; extended chains 1622−1639 cm^{-1}; intermolecular β-sheet 1612−1618 cm^{-1}).[45−48] Data were processed using OPUS software (Bruker), to subtract the water and water vapor contribution, and Origin software (OriginLab) for the curve fitting analysis.

Fabrication of BSA-MA Hydrogels. Freeze-dried BSA-MA (BSA-MA 1, BSA-MA 2, and BSA-MA 3) was dissolved at 10, 15, and 20% w/v in phosphate-buffered saline (PBS; pH 7.4; Gibco, Life Technologies). Photoinitiator 2-hydroxy-4′-(2-hydroxyethoxy)-2-methylpropiophenone (Irgacure 2959; Sigma-Aldrich), dissolved at 20% w/v in ethanol (EtOH) 70% v/v, was added to the BSA-MA solutions to a final concentration of 0.5% w/v. Hydrogel precursor solutions were cast into molds prepared by gluing silicone tubes (6 mm inner diameter) onto glass slides and photo-cross-linked by UV light irradiation (365 nm; 150 mW cm^{-2}; Bluewave 200 3.0 light-curing spot-lamp; Dymax) for 6 min.

For compression tests, 6 mL of each BSA-MA hydrogel precursor solution was cast into a 55 mm Petri dish, and hydrogel specimens (13 mm diameter, 2.4 mm height) were punched from the UV cured hydrogels (365 nm, 150 mW cm^{-2}, 6 min) and kept in PBS for 48 h before use.

Swelling of BSA-MA Hydrogels. Immediately after photo-cross-linking, BSA-MA bulk hydrogels were kept in PBS (pH 7.4) at 37 °C. After 72 h of incubation, the wet weight (W_{wet}) of each bulk hydrogel was measured. Hydrogels were then freeze-dried, and the dry weight (W_{dry}) of each hydrogel was also measured. The mass swelling ratio was calculated as the ratio between the hydrogel water uptake ($W_{\text{wet}} - W_{\text{dry}}$) and its dry weight ($W_{\text{dry}}$).

Mechanical Properties of BSA-MA Hydrogels. The mechanical properties of various BSA-MA hydrogels were studied using a dynamic mechanical analyzer (DMA; Q800; TA Instrument) in a controlled force mode. The hydrogels, in the equilibrium swollen state after 48 h in PBS, were clamped between a parallel-plate compression clamp, and a piece of Kimwipe (Kimtech Science; Kimberly-Clark Professional) around the samples was used to increase the grip on the hydrogels. BSA-MA scaffolds were compressed at a rate of 1 N min^{-1} from 0.01 N up to 12 N. The compressive modulus was calculated from the slope of the linear region of the stress−strain curve between 10% and 15% strain.

In Vitro Enzymatic Degradation of BSA-MA Hydrogels. Photo-cross-linked BSA-MA hydrogels were placed in PBS until reaching the equilibrium swelling, and then the wet weight of each sample was measured after its surface water was removed with a piece of Kimwipe. Each BSA-MA scaffold was then incubated in 0.5 mL of a 0.25% trypsin-EDTA (TE; Gibco, Life Technologies) solution at 37 °C in 5% CO_2. The enzyme solution was changed every 48 h. At predetermined time points t, the BSA-MA hydrogels were frozen at −80 °C overnight and lyophilized (FreeZone 4.5 L freeze-dryer; Labconco) for 48 h, and then the dry weight (W_{Dt}) of each sample was measured. The initial dry weight (W_{Di}) of each BSA-MA hydrogel was estimated from the ratio of the wet weight and the dry weight of control untreated hydrogels. Mass loss percentage was calculated according to the following formula:

$$\text{Mass loss } \% = 1 - \frac{W_{\text{Dt}}}{W_{\text{Di}}} \times 100$$

In Vitro Drug Release. Doxorubicin hydrochloride (Tocris Bioscience) was used for in vitro drug release studies. Photo-cross-linked BSA-MA hydrogels were placed in PBS until they reached the equilibrium swelling, and then they were incubated for 36 h at 4 °C in 1 mL doxorubicin solutions at molar ratios of 2:1 drug/BSA (180 μM, 271 μM, and 361 μM for BSA-MA hydrogels at 10%, 15%, and 20%

https://dx.doi.org/10.1021/acsabm.9b00984
ACS Appl. Bio Mater. 2020, 3, 920−934

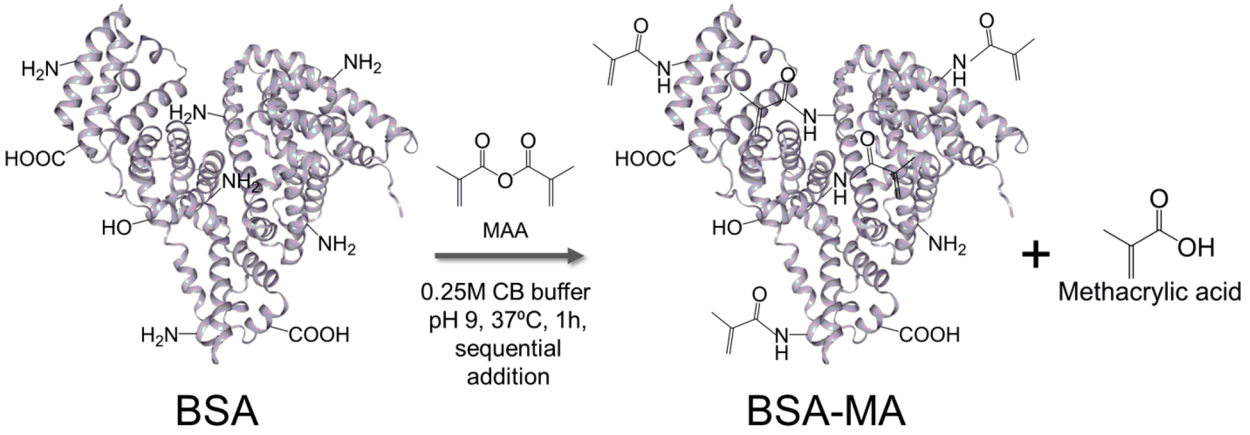

Figure 1. Synthesis of BSA-MA. Schematic illustration of the reaction between BSA and MAA. BSA, bovine serum albumin; MAA, methacrylic anhydride; CB, carbonate-bicarbonate; BSA-MA, BSA methacryloyl.

w/v, respectively) to allow adequate diffusion of the drug into the hydrogels. Afterward, the doxorubicin solution was replaced with 1 mL of PBS (pH 7.4; Gibco, Life Technologies), and its absorbance at 484 nm was measured with a microplate reader (Infinite M200 Pro; Tecan AG) to determine the mass of the doxorubicin loaded into the hydrogels ($M_{DOX\text{-}Enc}$). Encapsulation efficiency was calculated as Encapsulation efficiency % = $(M_{DOX\text{-}added}/M_{DOX\text{-}Enc}) \times 100$ and drug loading as Drug loading = $M_{DOX\text{-}Enc}/(M_{DOX\text{-}Enc} + M_{BSA\text{-}MA}) \times 100$, where $M_{DOX\text{-}added}$ is the mass of doxorubicin added and $M_{BSA\text{-}MA}$ is the mass of BSA in the BSA-MA hydrogels. At determined time points, PBS was collected and replaced with 1 mL of fresh PBS, and its absorbance at 484 nm was measured using a microplate reader to determine the drug concentration in the solution and consequently the drug release profile over time. Doxorubicin solutions at different molar concentrations were used to obtain the standard curve used for calculating the cumulative drug release.

Cytocompatibility of BSA-MA Hydrogels. Cytocompatibility of BSA-MA hydrogels was evaluated by culturing human hepatocellular carcinoma cells (Huh-7.5; Apath) as a model cell in a 2D BSA-MA environment. BSA-MA 1, 2, and 3 were dissolved at 15% w/v in PBS, with 0.5% w/v photoinitiator Irgacure 2959 (a stock solution dissolved at 20% w/v in EtOH 75% v/v). BSA-MA solutions were then cast in 48-well plates (0.2 mL/well) and photo-cross-linked via UV light (365 nm; 100 mW cm^{-2}; 6 min), and the obtained gels were washed with PBS. Huh-7.5 cells were cultured in high glucose Dulbecco's modified Eagle's medium (DMEM; Gibco, Life Technologies) containing sodium pyruvate and L-glutamine and supplemented with 10% fetal bovine serum (FBS; Gibco, Life Technologies) and 1% antibiotic-antimycotic (Gibco, Life Technologies) in a humified atmosphere at 37 °C in 5% CO_2. Huh-7.5 cells of 3×10^4 were seeded on top of each BSA-MA gel and cultured for 5 days. Media were changed every 2 days. Cells seeded on a 2D 48-well tissue culture plate (TCP) were used as control. Cell viability was assessed every other day using a Live/Dead Cell Viability/Cytotoxicity kit (Life Technologies) according to manufacturer's instructions. Briefly, 4 μM calcein-acetomethoxy (calcein-AM) and 8 μM ethidium homodimer-1 (EthD-1) in 0.5 mL of culture media were added to each well and incubated at 37 °C in 5% CO_2 for 1 h. Live and dead cells, stained green and red, respectively, were imaged using an LSM710 confocal microscope equipped with an Axio Observer Z1 inverted microscope. Images were processed using ImageJ software. Cell viability was also assessed using the Cell Counting Kit-8 (CCK-8; Dojindo Molecular Technologies) assay according to the manufacturer's instructions. Each well was incubated with a CCK solution (350 μL; 1:10 CCK to culture medium) at 37 °C in 5% CO_2 for 2 h, and the absorbance at 450 nm was measured using an Infinite 200 PRO microplate reader (Tecan).

Encapsulation of Huh-7.5 Cells within BSA-MA Hydrogels and Evaluation of Their Viability, Functionality, and Morphology. BSA-MA 3 and poly(ethylene glycol)diacrylate (PEGDA; MW 4600) were dissolved at 10%, 15%, and 20% w/v in PBS, and the photoinitiator Irgacure 2959, predissolved at 20% w/v in EtOH 75% v/v, was added to a final concentration of 0.1% w/v. The hydrogel precursor solutions were filtered (0.2 μm) and added to the cell suspensions. Then 50 μL of a hydrogel precursor solution containing 2×10^5 Huh-7.5 cells was cast into sterile silicone tube molds (6 mm inner diameter) and UV cured with UV light (365 nm; 20 mW cm^{-2}; Bluewave 200 3.0 light-curing spot-lamp; Dymax) for 3 min. Cell-laden hydrogels were transferred from the molds into 48-well plates and immediately incubated in 1 mL of complete media at 37 °C in 5% CO_2. Media were changed every 3 days, and encapsulated cells were cultured up to 1 week. Cells encapsulated in PEGDA hydrogels were used as a control group. PEGDA was synthesized as previously reported.[49] Its degree of acrylation was 74.08% (Figure S2).

Encapsulation efficiency was calculated by counting the number of cells released into the culture media 24 h after encapsulation. The viability of encapsulated cells was assessed using the Cell Counting Kit-8 (CCK-8; Dojindo Molecular Technologies) and the Live/Dead Cell Viability/Cytotoxicity kit (Life Technologies), according to manufacturers' instructions. For CCK-8 measurements, each hydrogel was incubated with 0.5 mL of a CCK solution (a 1:10 CCK-to-culture medium) at 37 °C in 5% CO_2 for 4 h, and the absorbance at 450 nm was measured using an Infinite 200 PRO microplate reader (Tecan). For Live/Dead analysis, each hydrogel was incubated with 0.5 mL of culture media with 4 μM calcein-acetomethoxy (calcein-AM) and 8 μM ethidium homodimer-1 (EthD-1) at 37 °C in 5% CO_2 for 1 h. Hydrogels were washed with PBS before images of live cells (stained green), and dead cells (stained red) were taken using an LSM710 confocal microscope equipped with an Axio Observer Z1 inverted microscope. Images were processed using ImageJ software.

The functionality of encapsulated Huh-7.5 cells was evaluated by determining the amount of albumin secreted into the culture media within a 24 h period using a human albumin enzyme-linked immunosorbent assay (ELISA) kit (Abcam).

Morphology of encapsulated cells was evaluated through scanning electron microscopy (SEM). Hydrogels were fixed with paraformaldehyde (4% PFA; Alfa Aesar) for 30 min, washed twice with PBS, longitudinally cut, sequentially dehydrated with a series of EtOH (25%, 50%, 75%, 95%, and 100% v/v; 30 min each), frozen overnight at −80 °C, and lyophilized for 48 h (FreeZone 4.5 L freeze-dryer; Labconco). Before the images were aquired with a FESEM 7600F (JEOL) at 5 kV and different magnifications, the surface of the freeze-dried hydrogels was coated with a 10 nm platinum film in a JFC-1600 sputter coater (20 mA, 60 s; JEOL).

Statistical Analysis. Prism software (GraphPad version 7.0) was utilized to analyze the data unless otherwise specified. Triplicate samples for each condition, unless otherwise specified, were used, and results are shown as mean ± standard deviation (SD). Statistical differences between groups were evaluated using one-way analysis of

https://dx.doi.org/10.1021/acsabm.9b00984
ACS Appl. Bio Mater. 2020, 3, 920−934

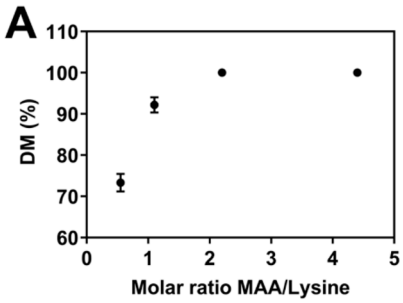

Sample	Molar ratio MAA / Lys	mmol Lys / g BSA	Unreacted Lys groups	DM (%)
BSA	0	0.445 ± 0.014	29.6	**0**
BSA-MA 1	0.55	0.119 ± 0.009	7.9	**73.31 ± 2.11**
BSA-MA 2	1.1	0.035 ± 0.008	2.3	**92.18 ± 1.85**
BSA-MA 3	2.2	0	0	**100.00**
BSA-MA 4	4.4	0	0	**100.00**

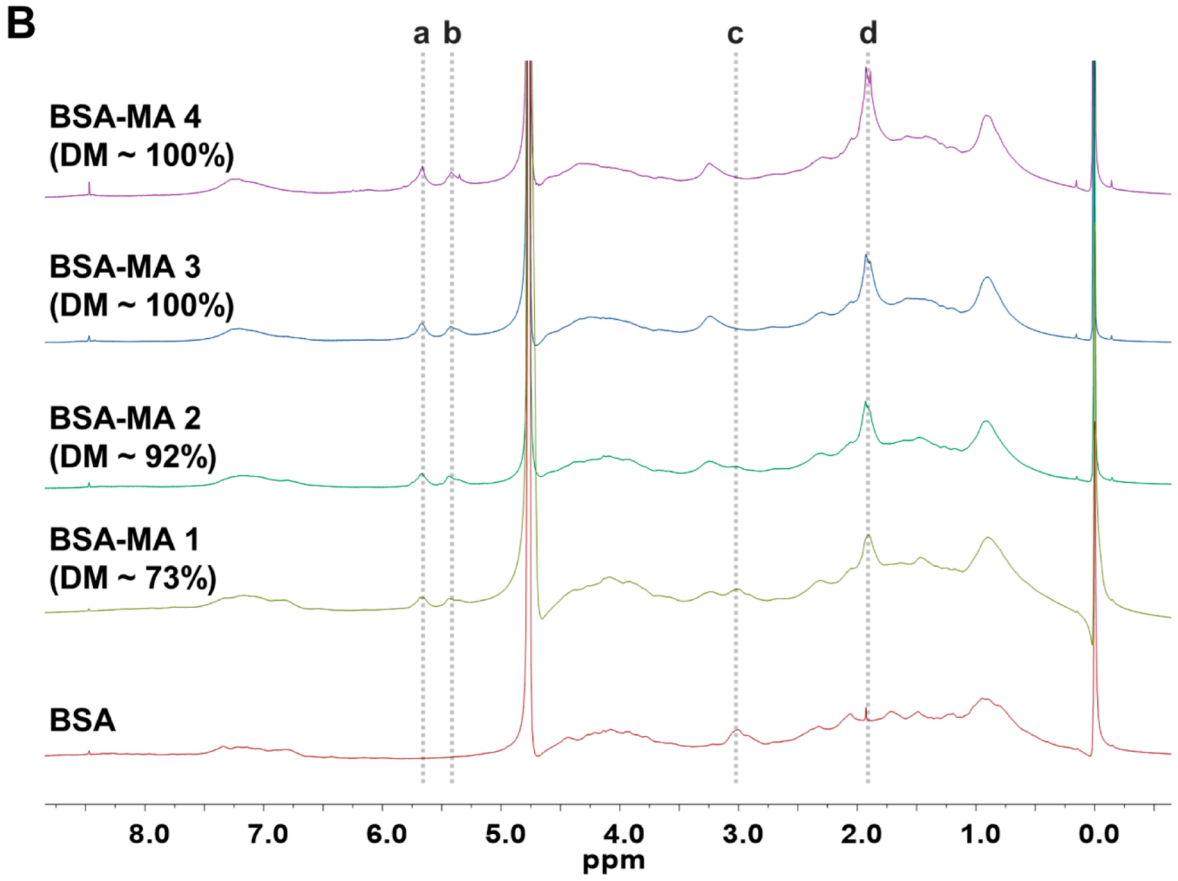

Figure 2. Degree of methacryloylation (DM) of BSA-MA. (A) Degree of methacryloylation (DM) of the four BSA-MA samples synthesized (right) and the relationship between the feed molar ratio of MAA/Lysine groups and the resulting DM% of the synthesized BSA-MA (left). DM% was quantified using the TNBS assay. Data are reported as mean ± SD (n = 3). By increasing the amount of MAA used, BSA-MA samples with increasing DM% values until complete functionalization of all the sterically available lysine groups. The point corresponding to unfunctionalized BSA (BSA, DM% ≈ 0%, molar ratio MAA/Lys = 0) is not reflected in the graph on the left to better discern the points corresponding to the different BSA-MA samples. (B) ^{1}H NMR spectra of BSA and BSA-MA samples with different degrees of methacryloylation. (a, b) Acrylic protons of methacrylamide grafts (5.4 and 5.7 ppm); (c) methylene protons of unreacted lysine groups (at around 3.0 ppm); (d) methyl protons of methacrylamide grafts (at around 1.9 ppm). The peak at 0 ppm corresponds to the internal standard TMSP.

variance (ANOVA) followed by either Sidak's or Tukey's test for multiple comparisons. Results with a p-value of 0.05 or below were considered statistically significant.

RESULTS AND DISCUSSION

Synthesis of BSA-MA with Different Degrees of Methacryloylation. BSA-MA was synthesized via the direct reaction between MAA and the free lysine amino groups in the BSA molecule (Figure 1). BSA was dissolved into a carbonate-bicarbonate (CB) buffer, and the pH of the solution was kept above the BSA isoelectric point (BSA IEP = 4.7),[50] thus to reduce the number of protonated free amino groups that would not react with MAA.[40] By varying the molar ratio of MAA to lysine groups (0.55, 1.1, 2.2, and 4.4 for BSA-MA 1, BSA-MA 2, BSA-MA 3, and BSA-MA 4, respectively), we successfully synthesized four BSA-MA with different degrees of methacryloylation (DM% ≈ 73.3% (BSA-MA 1), DM% ≈ 92.2% (BSA-MA 2) and DM% ≈ 100% for (BSA-MA 3) and (BSA-MA 4)), as calculated by TNBS assay (Figure 2A and Figure S1), and with yields above 87% under the reaction conditions used (Table 1). In particular, by increasing the amount of MAA used, BSA-MA samples with increasing DM% values were achieved until saturation of the free amino groups available for the reaction was reached (e.g., BSA-MA 3 and BSA-MA 4).

https://dx.doi.org/10.1021/acsabm.9b00984
ACS Appl. Bio Mater. 2020, 3, 920−934

Table 2. Content of BSA Amino Acids with Side Groups of Particular Interest for Functionalization[a]

amino acid (AA)	reactive group	content (AA/molecule BSA)	content (%)[b]	molar mass (g/mol)	mmol/g BSA[c]	mmol/g BSA in literature
lysine	$-NH_2$	59[50,54]	10.1%	146.19	0.888	0.84[55]
hydroxylysine	$-NH_2$; −OH	NP[54]	0%	162.187	NA	NA
hydroxyproline	−OH	NP[54,56]	0%	131.13	NA	NA
threonine	−OH	33[54]	5.6%	119.12	0.495	0.503[57]
tyrosine	−OH	20[50,54]	3.4%	181.19	0.301	0.154;[57] 0.26[55]
serine	−OH	28[50,54]	4.8%	87	0.421	0.450[57]
cysteine	−SH	35[#,50,54]	6%	121.16	0.527	0.171;[57] 0.07[55]

[a]NP: Not present. NA: Not available. [b]Based on BSA containing 583 AA. [c]Based on BSA MW = 66.4 kDa. [d]Thirty-four of these cysteines are involved in the formation of 17 disulfide bridges.[50]

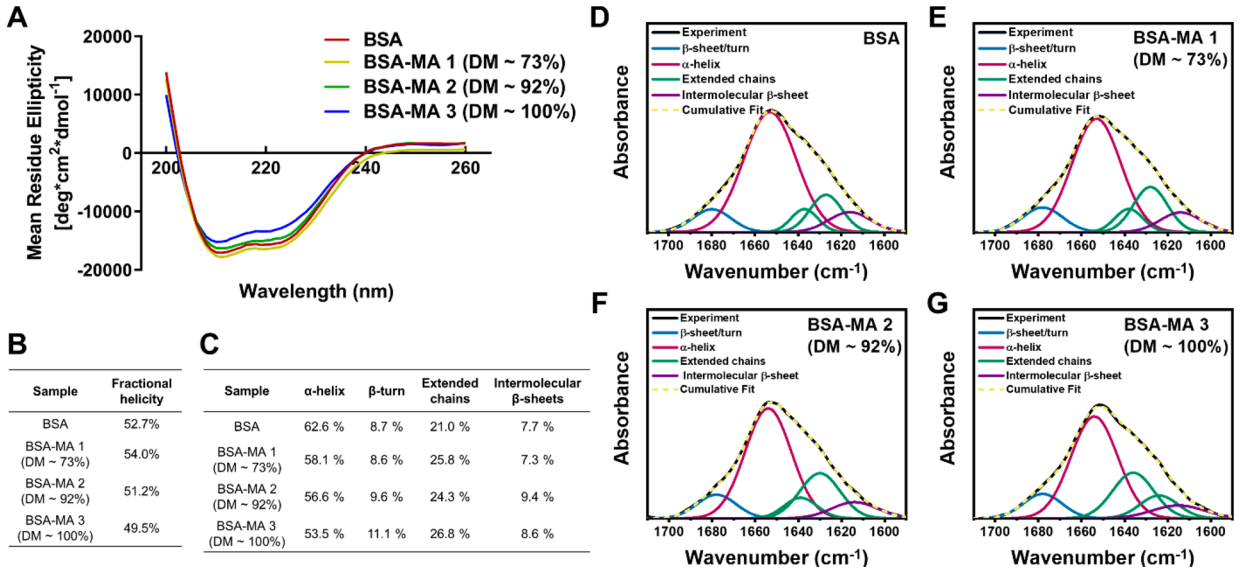

B

Sample	Fractional helicity
BSA	52.7%
BSA-MA 1 (DM ~ 73%)	54.0%
BSA-MA 2 (DM ~ 92%)	51.2%
BSA-MA 3 (DM ~ 100%)	49.5%

C

Sample	α-helix	β-turn	Extended chains	Intermolecular β-sheets
BSA	62.6 %	8.7 %	21.0 %	7.7 %
BSA-MA 1 (DM ~ 73%)	58.1 %	8.6 %	25.8 %	7.3 %
BSA-MA 2 (DM ~ 92%)	56.6 %	9.6 %	24.3 %	9.4 %
BSA-MA 3 (DM ~ 100%)	53.5 %	11.1 %	26.8 %	8.6 %

Figure 3. Secondary structure of BSA and BSA-MA samples. (A) CD spectra of BSA and BSA-MA in DI H_2O. (B) Fractional helicity percentage of BSA and BSA-MA samples, as calculated from the CD spectra shown in (A). Data reported are mean values (n = 3). (C) Secondary structure fractions (%) of BSA and BSA-MA samples calculated from the deconvoluted ATR-FTIR spectra shown in D−G. Data are reported as mean values (n = 3). (D−G) Normalized ATR-FTIR spectra of (D) native BSA, (E) BSA-MA 1, (F) BSA-MA 2, and (G) BSA-MA 3. The contribution of α-helix (dark red), β-turn (blue), extended chains (green), and intermolecular β-sheets (purple) were assigned on the basis of previously reported values.[45−48] Black lines represent the experimentally obtained spectra. Yellow dashed lines represent the cumulative fit of the component curves.

Although the TNBS assay allows for precise quantification of the free primary amines in proteins and in turn, accurately quantified methacrylamide groups, it does not provide visible information about the presence of impurities (e.g., methacrylic acid byproduct) or the presence of methacrylate functions. Therefore, we also evaluated the methacryloylation of each sample through ^{1}H NMR. Compared to the BSA spectrum, BSA-MA spectra contain specific peaks at around 5.4 and 5.7 ppm, corresponding to the acrylic protons of the methacrylamide grafts, and at approximately 1.9 ppm, corresponding to the methyl protons of the methacrylamide grafts. The presence and different intensities of these peaks (Figure 2B) indicate the successful conjugation of different amounts of MAA to the BSA amino groups. Conversely, the intensity of the peak at around 3.0 ppm, corresponding to the methylene protons of unreacted lysine residues, decreases with increasing DM, up to complete disappearance in the spectra of BSA-MA with DM ≈ 100% (BSA-MA 3 and BSA-MA 4), indicating complete reaction of MAA with the available free amino groups in BSA. The peak of the methylene protons of lysine was shifted from around 3.0 ppm to 3.2 ppm as the degree of methacryloylation increased. Also, impurities were marginally visible only in the BSA-MA 4 sample spectrum, as indicated by peaks corresponding to the methacrylic acid byproduct (at around 5.3 and 1.8 ppm).

MAA could react with both amine groups (mainly from the lysine and hydroxylysine residues) and hydroxyl groups (from hydroxyproline, threonine, serine, tyrosine, and hydroxylysine residues), resulting in the formation of both methacrylamide and methacrylate functions, respectively, though the former was the dominant form in methacrylated proteins such as gelMA or methacrylated tropoelastin (MeTro).[41,51,52] Additionally, Claaßen et al., when analyzing the ^{1}H−^{13}C heteronuclear single quantum coherence (HSQC) NMR spectra of gelMA containing both methacrylate and methacrylamide groups, found that among all the amino acids bearing a reactive hydroxyl group in the side chain, only the signals of hydroxyproline and hydroxylysine presented a shift in the spectra upon methacryloylation, indicating that only these residues reacted with MAA.[41] Also, it has been highlighted that methacrylate functionalization occurred only when a higher molar ratio of MAA to lysine groups (e.g., 4.4:1, 5:1, and 10:1) was adopted.[41,51] In our study, BSA-MA 3 and BSA-MA 4 possess a similar DM based on TNBS results, though a double feed molar ratio of MAA was used for the synthesis of BSA-MA 4. Therefore, the exceeding molar ratio of MAA used for BSA-MA 4 might result in the formation of a

https://dx.doi.org/10.1021/acsabm.9b00984
ACS Appl. Bio Mater. 2020, 3, 920−934

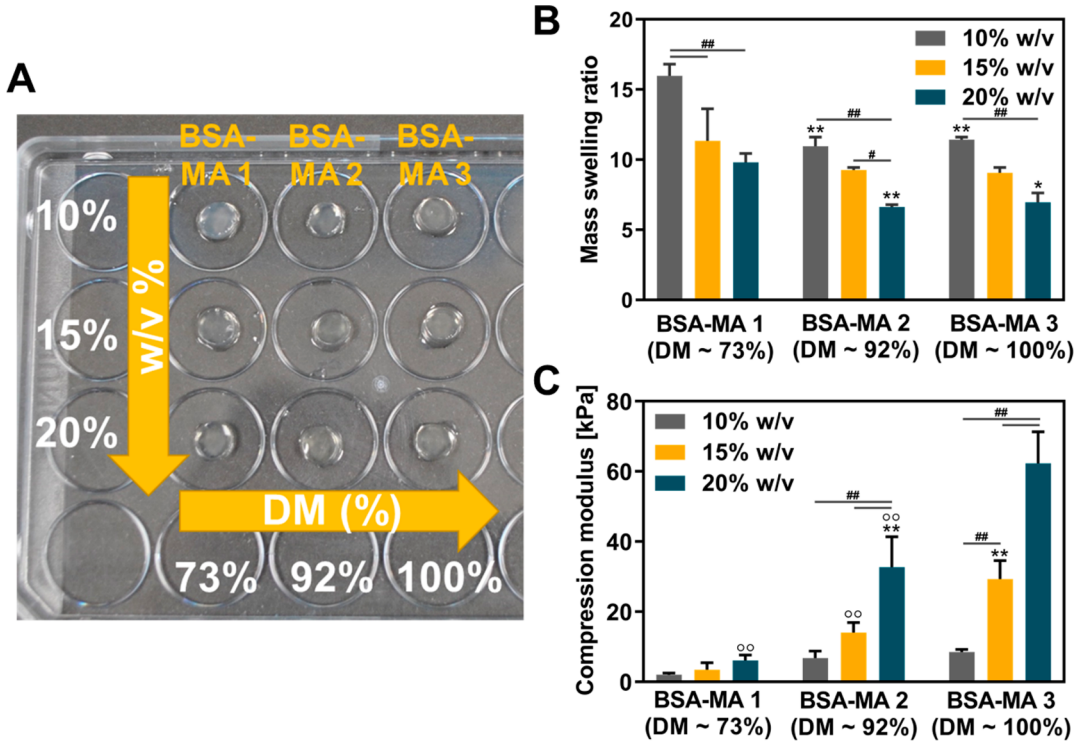

Figure 4. Physicochemical properties of BSA-MA bulk hydrogels. (A) Gross images of BSA-MA hydrogels. (B) Mass swelling of BSA-MA hydrogels in PBS. Data are reported as mean ± SD (n = 3). ∗: $p < 0.05$, ∗∗: $p < 0.01$, as compared to BSA-MA 1 same w/v%. #: $p < 0.05$, ##: $p < 0.01$, between the samples at the extremities of the line. (C) Compression modulus of BSA-MA hydrogels. Data are reported as mean ± SD (n = 4). ∗∗: $p < 0.01$, as compared to BSA-MA 1 same w/v %. ○○: $p < 0.01$, as compared to BSA-MA 3 same w/v %. ##: $p < 0.01$, between the samples at the extremities of the line.

few methacrylate groups. In the ^{1}H NMR spectra of gelMA, the peaks of the methacrylate groups (around at 1.9, 5.7, and 6.1 ppm) are reported to appear very close to those belonging to the methacrylamide groups.[41,52,53] The specific peak of the methacrtylate groups at 6.1 ppm seemed little visible in the ^{1}H NMR spectra of all the BSA-MA samples synthesized, although the broad peaks of BSA make it difficult to differentiate the resonance peaks corresponding to the methacrylamide and methacrylate functions. The lack of methacrylate functions in the highly substituted BSA-MA samples (BSA-MA 3 and BSA-MA 4), as well as in the BSA-MA 1 and 2 samples, might be closely related to the amino acid content of BSA (Table 2), which does not possess any hydroxyproline or hydroxylysine groups.

Of note, although the TNBS assay provides precise information about the free primary amino groups, the molar content of lysine groups of BSA molecules as calculated from the TNBS data was almost half of the molar content reported in the literature.[50,55] The native globular conformation of BSA might account for this discrepancy, as in the other studies;[50,55] the molar content was calculated based on cDNA, mass spectrometry, and amino acid sequence data.

Because of the slight presence of impurities in the BSA-MA 4 sample, only BSA-MA 1, BSA-MA 2, and BSA-MA 3 were selected for subsequent experiments and analyses.

Secondary Structure of BSA-MA. To evaluate the effect of the methacryloyl functionalization on the structural conformation of the BSA molecules, the secondary structure of the BSA-MA samples was investigated. The CD spectra of native BSA possess two negative bands at 208 and 222 nm typical of proteins with an α-helical structure (Figure 3A).[42] The CD spectra of BSA-MA resemble that of native BSA, though the insertion of methacryloyl groups led to a slight change in the intensity of the two negative bands, suggesting a marginal reduction in the α-helix content of the BSA molecules upon methacryloylation, especially in the sample with the highest degree of functionalization (BSA-MA 3). Indeed, CD measurements show that the fractional helicity value of BSA-MA 3 (49.5%) is slightly lower than those of native BSA (52.7%) and BSA-MA with a lower degree of functionalization (54% and 51.2% for BSA-MA 1 and BSA-MA 2, respectively) (Figure 3B).

FTIR deconvoluted absorbance spectra of BSA (Figure 3D) and BSA-MA (Figure 3E−G) samples were consistent with the CD results. These spectra show a progressive reduction in the intensity of the band around 1653−1654 cm^{-1}, representative of the α-helix content (62.6% for BSA and 58.1%, 56.6%, and 53.5% for BSA-MA 1, 2, and 3, respectively; Figure 3C), and a simultaneous increase in the intensity of the bands around 1622 and 1639 cm^{-1}, representative of the extended chain content (21% for BSA; 25.8%, 24.3%, and 26.8% for BSA-MA 1, 2 and 3, respectively; Figure 3C), with the increase of protein methacryloylation. Indeed, since the majority (73%) of the lysine amino groups reside in the α-helical region of the BSA protein,[58] the incorporation of methacrylamide groups might sterically interfere with the helix backbone as well as alter the hydrogen bonding patterns between the carbonyl oxygen and the amide hydrogen of the protein main chain, resulting in partial unfolding of the α-helical secondary structure, primarily when a higher degree of methacryloylation were employed. However, the fact that the overall shape of the amide I band remains unchanged despite the different DM

https://dx.doi.org/10.1021/acsabm.9b00984
ACS Appl. Bio Mater. 2020, 3, 920−934

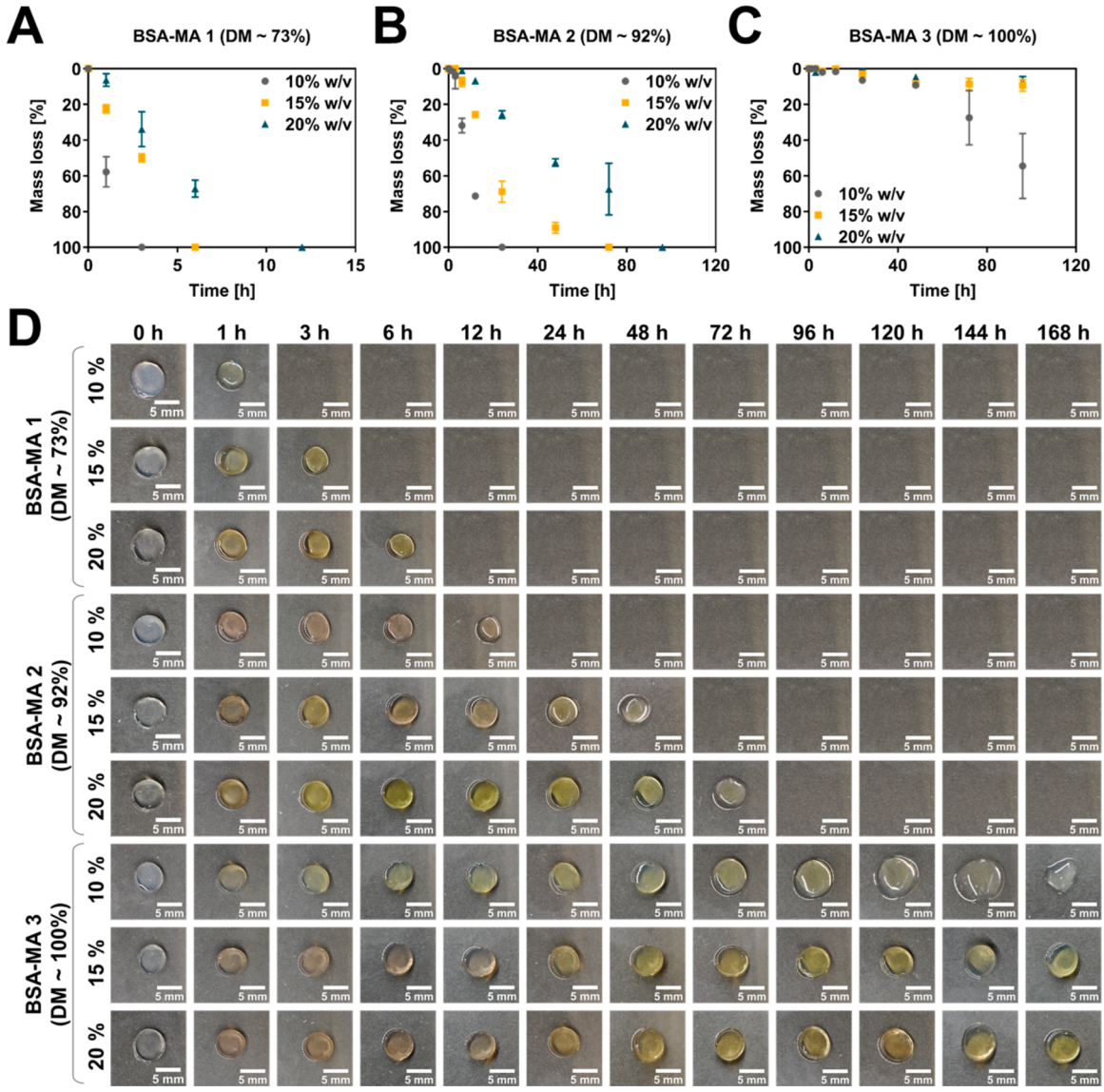

Figure 5. Enzymatic degradation of BSA-MA hydrogel disks. (A–C) Mass loss of (A) BSA-MA 1, (B) BSA-MA 2, and (C) BSA-MA 3 hydrogels. Data are reported as mean ± SD (n = 3). (D) Overall morphology of BSA-MA hydrogels (scale bar = 5 mm). The degradation rate was dependent on the DM and mass concentration.

suggests that all the methacryloylated samples maintain the α-helix secondary structure similar to BSA. The percentage of β-turns and intermolecular β-sheets, instead, seems to be less affected by the functionalization process, compared to that of α-helix (Figure 3C).

Physicochemical Properties of BSA-MA Bulk Hydrogels. BSA-MA (BSA-MA 1, BSA-MA 2, and BSA-MA 3) solutions at different concentrations (10%, 15%, and 20% w/v) were successfully photo-cross-linked (with an intensity of 150 mW cm^2 and for 6 min at 365 nm). Obtained transparent hydrogels disks (with 6 mm in diameter and 2 mm in thickness in Figure 4A) were subsequently characterized including swelling behavior, mechanical properties, and degradation rate, respectively.

All the BSA-MA hydrogels reached equilibrium swelling within 1 to 4 h, irrespective of the protein concentration and the DM. The mass swelling of BSA-MA hydrogels in PBS (Figure 4B), defined as the ratio between the hydrogel water uptake and its dry weight, decreased with the increase of BSA-MA concentration and the degree of methacryloylation, which is in agreement with what was previously reported with other UV photo-cross-linked polymer-based hydrogels.[53,59−61] Indeed, a higher number of cross-linkable groups resulted in a higher cross-linking density, and thus in a tighter less-flexible network that was less able to take up water molecules. Additionally, a higher degree of methacryloylation reduced the number of free polar amino groups, which represent the main sites of water−protein interactions, thus decreasing the water-binding capacity of BSA molecules.[59]

The mechanical properties of BSA-MA hydrogels were evaluated through compression analysis. The compression modulus (Figure 4C) of BSA-MA hydrogels ranged from a few kPa to 60 kPa, depending on the protein concentration and the degree of methacryloylation. In particular, the compression modulus increased with increasing the BSA-MA content and DM, indicating the presence of a tighter network under these conditions, which is inversely related to what was observed for the swelling. BSA-MA samples showed nonlinear stress−strain

https://dx.doi.org/10.1021/acsabm.9b00984
ACS Appl. Bio Mater. 2020, 3, 920−934

A

Sample	w/v %	Encapsulation efficiency %	Drug loading
BSA-MA 1 (DS ~ 73%)	10%	71.78 ± 6.08	0.0138 ± 0.0011
	15%	84.07 ± 2.97	0.0151 ± 0.0005
	20%	86.89 ± 1.09	0.0167 ± 0.0002
BSA-MA 2 (DS ~ 92%)	10%	87.13 ± 2.83	0.0167 ± 0.0005
	15%	88.70 ± 0.80	0.0160 ± 0.0001
	20%	90.40 ± 0.38	0.0173 ± 0.0000
BSA-MA 3 (DS ~ 100%)	10%	85.43 ± 1.27	0.0164 ± 0.0002
	15%	87.21 ± 1.38	0.0157 ± 0.0002
	20%	88.79 ± 1.52	0.0170 ± 0.0003

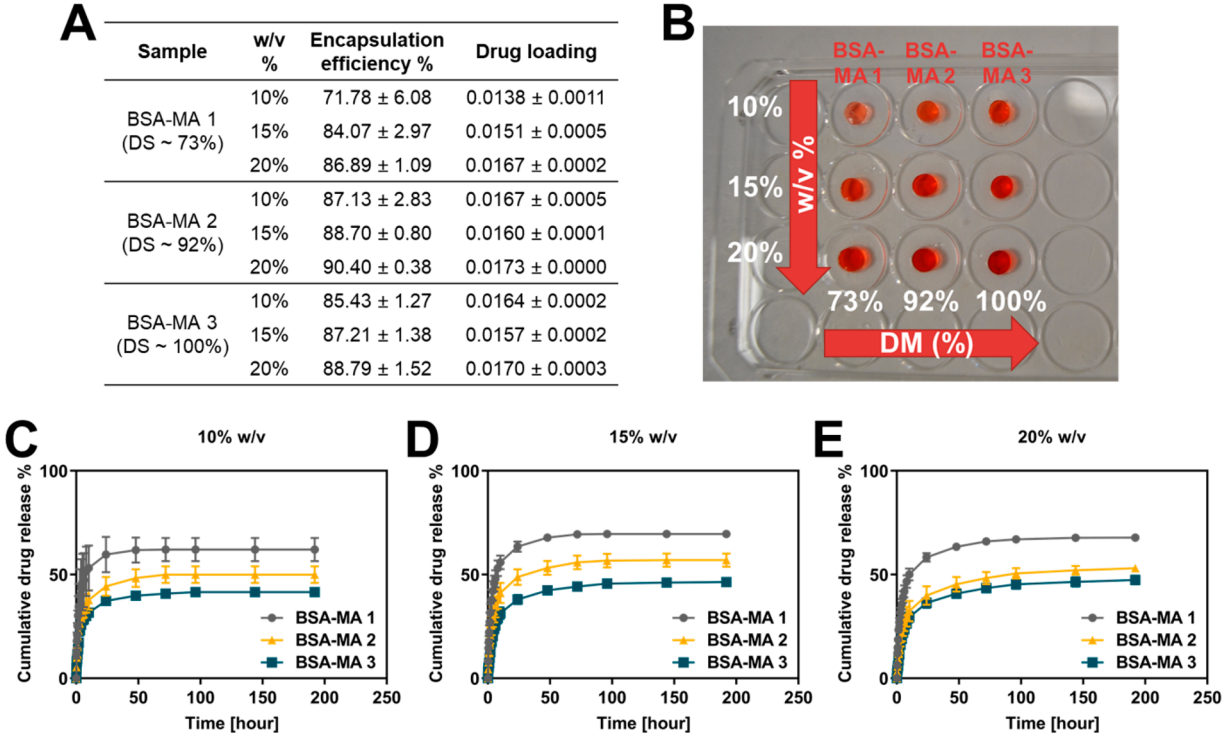

Figure 6. Loading and release profiles of doxorubicin from BSA-MA 1, 2, and 3 hydrogels prepared at different protein concentrations. (A) Drug loading and encapsulation efficiency percentage of doxorubicin into BSA-MA hydrogels. (B) Gross images of BSA-MA hydrogels loaded with doxorubicin after 196 h in PBS. (C–E) Cumulative drug release percentage of doxorubicin from BSA-MA hydrogels at (C) 10% w/v, (D) 15% w/v, and (E) 20% w/v. Data are reported as mean ± SD (n = 3).

curves (Figure S3), with a strain stiffening behavior typical of cross-linked natural-polymer based hydrogels.[62,63]

The capability of tuning a wide range of mechanical properties by merely modifying few parameters, such as the polymer concentration and the degree of modification, makes BSA-MA a photocurable protein-based material of particular interest to generate functional tissues or cancer models in vitro, as many studies have shown that cell behavior is highly dependent on the scaffold stiffness.[64−66] For instance, human mesenchymal stem cells (hMSC) cultured on collagen type I-coated polyacrylamide gels of various stiffnesses (0.1, 1, 11, and 34 kPa) committed to the lineage dictated by the substrate elasticity toward either neurons, myoblasts, or osteoblasts.[64] Also, various carcinoma cells, when encapsulated in PEGDA hydrogels of different stiffness (2−70 kPa), exhibited proliferation, cell aggregation, and gene expression patterns that were strongly correlated to the hydrogel compressive modulus.[65]

Hydrogel biodegradation is an essential feature of biomedical applications that requires complete resorption or dissolution in vivo.[67] Albumin molecules are proteolytically degraded in ubiquitous tissues inside the body, and trypsin and pepsin among the various proteases have been reported to be the most effective enzymes in cleaving BSA molecules in vitro.[50] Therefore, the enzymatic degradation of BSA-MA hydrogels was evaluated using trypsin (0.25%). The degradation rate of BSA-MA hydrogels appears to be strongly dependent on the BSA-MA concentration and DM (Figure 5). In particular, the higher the DM or the protein concentration, the slower the degradation, with BSA-MA 1 hydrogels being completely disintegrated within 12 h (Figure 5A,D) and BSA-MA 3 hydrogels at 15% and 20% w/v losing less than 10% of their mass after 96 h (Figure 5C). In all the BSA-MA hydrogels, except BSA-MA 3 15% and 20% w/v, overall changes in the gel shape (size reduction) in a time- and concentration-dependent manner were observable (Figure 5D), suggesting a combinatorial surface and bulk erosion degradation mechanism. BSA-MA 3 15% and 20% w/v, instead, maintained almost entirely their integrity for 1 week, suggesting that tightly cross-linked network of these gels could restrict the enzyme diffusion within the constructs and that BSA MA hydrogels with more cross-linking bridges made of C−C bonds owing to a higher DM and higher concentration could be less reactive to enzymes.

Since the degradation of scaffolds used in tissue engineering should match the cells' time to remodel their surroundings, BSA-MA hydrogels with controllable degradation can be utilized for the fabrication of constructs for a wide array of regenerative medicine applications, although it should be kept in mind that the in vitro degradation rates reported in this study are not representative of the actual in vivo degradation rates since the latter ones depend on the in vivo local microenvironments.

In Vitro Drug Release. Doxorubicin, an anthracycline antibiotic widely used for the treatment of various types of cancers, was chosen as a model drug. Doxorubicin was loaded into swollen BSA-MA hydrogels with efficiencies above 84% for all the hydrogels, except for BSA-MA 1 hydrogels at 10% w/v, of which the encapsulation efficiency was around 71%, probably due to the loose polymeric network less able to retain the drug (Figure 6A). For all the hydrogels, the drug release rate was initially rapid, with the majority of drug released within 8 h, and then slowly reached a plateau (Figure 6C−E), with the time necessary to reach this steady state correlated to

https://dx.doi.org/10.1021/acsabm.9b00984
ACS Appl. Bio Mater. 2020, 3, 920−934

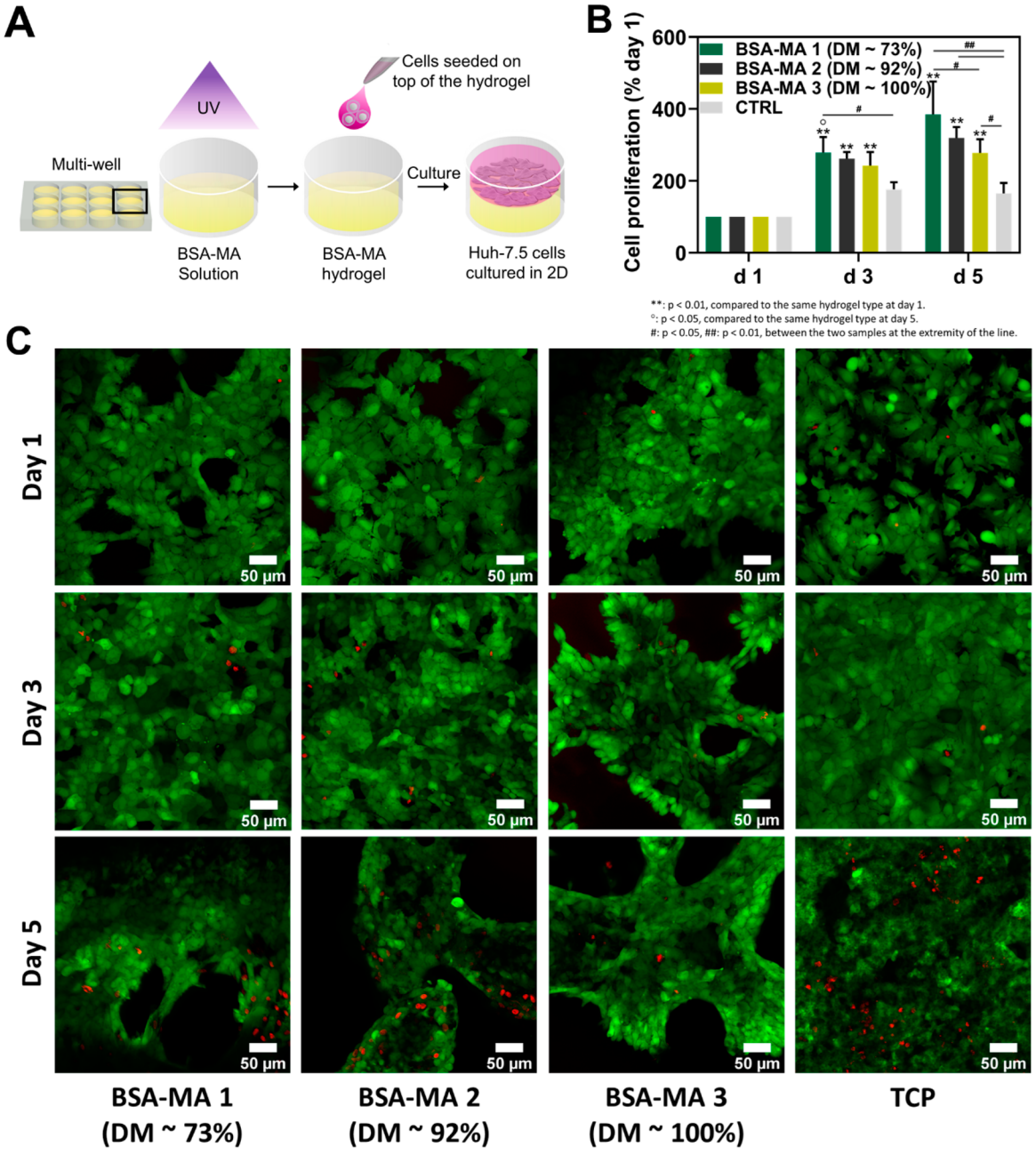

Figure 7. Cytocompatibility of BSA-MA hydrogels. Human hepatocellular carcinoma (Huh-7.5) cells were seeded on top of preformed BSA-MA gels with different degrees of methacryloylation and cultured in such a 2D environment for 5 days. (A) Schematic illustration. (B) Cell proliferation was determined using the CCK-8 assay. Absorbance values of each group were normalized to day 1 values of the same group. Results are reported as mean ± SD (n = 3). (C) Cell viability was qualitatively assessed using the Live/Dead assay kit. Live cells were stained green using calcein-AM, and dead cells were stained red using EthD-1. Images were taken using a confocal microscope with a 20× lens. Scale bar is 50 μm. TCP, tissue culture plates.

the BSA-MA concentration (~24 h for hydrogels at 10% w/v, ~48 h for hydrogels at 15% w/v, and ~72 h for hydrogels at 20% w/v). As previous works reported that doxorubicin strongly binds to albumin molecules via hydrophobic and hydrophilic interactions stabilized by H-bonds and involving several amino acids,[68] this initial rapid release might be mainly due to the diffusion of the unbound drug. For all the hydrogels prepared at the same protein concentration, drug release was the higher as the lower was the degree of methacryloylation, probably as a result of the drug binding abilities of BSA and the higher cross-linking density associated with a higher degree of methacryloylation. The complexation of doxorubicin to BSA molecules in a tighter polymeric network (e.g., BSA-MA 3) might block the diffusion of unbound drug molecules in the solution diffused into the hydrogel core. However, in none of the hydrogels was the loaded doxorubicin completely released (Figure 6B), and between ~40% (for BSA-MA 1) and ~60% (for BSA-MA 3) of the drug remained inside the hydrogels, most probably due to strong interactions between doxorubicin and BSA. Additionally, as visible from the red colored BSA-MA hydrogels in Figure 6B, doxorubicin penetrated throughout all the hydrogel matrices, and, as doxorubicin (MW ≈ 579.99 g/mol) is larger than glucose (~180 g/mol) and oxygen, diffusion of small molecules and gas molecules within the

https://dx.doi.org/10.1021/acsabm.9b00984
ACS Appl. Bio Mater. 2020, 3, 920−934

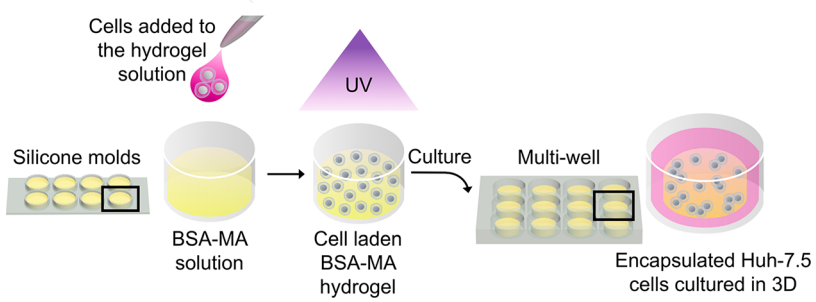

Figure 8. Schematic illustration of the cell encapsulation process.

polymeric network should not be hampered in any of the BSA-MA hydrogels.

Cytocompatibility of BSA-MA Hydrogels and Encapsulation of Huh-7.5 Cells within BSA-MA Hydrogels. Although albumin does not possess the cell-adhesion sequences found in collagen, laminin, or fibrinogen (e.g., RGD sequence), various cell types have shown to bind albumin molecules, either in their native or refolded conformation.[21] For instance, the presence of the albondin 60 kDa glycoprotein (gp60) on the plasma membrane of continuous endothelium and alveolar epithelium[22] empowered electrospun albumin scaffolds to support the adhesion and growth of endothelial cells.[30] Protein receptors for albumin molecules (e.g., heterogeneous nuclear ribonucleoproteins and calreticulin) have also been found in the plasma membrane of various human cancer cell lines.[21] On the other hand, attachment of cardiomyocytes to electrospun albumin scaffolds has been hypothesized to be favored by the binding of serum adhesive proteins such as laminin.[32]

We further investigated cellular responses inside photocurable BSA-MA hydrogel scaffolds using Huh-7.5 as model cells. To first evaluate whether our BSA-MA hydrogels could be cytocompatible for liver cells, Huh-7.5 cells were seeded on top of preformed BSA-MA gels with different degrees of methacryloylation and cultured in such a two-dimensional (2D) environment for 5 days (Figure 7A). Interestingly, cells were attached to and spread on the surface of all the BSA-MA gels, remaining viable throughout the entire culture period, as observed from the Live/Dead fluorescent images (Figure 7C) and the CCK-8 data (Figure 7B). Cell proliferation increased progressively from day 1 to day 5 when cells were cultured on 2D BSA-MA substrates, while it increased until day 3 and then decreased slightly at day 5 when cells were cultured in standard tissue culture plates, probably due to space limitation (Figure 7B). Indeed, cells cultured on TCP substrata seem to have reached confluency at day 5, and more dead cells were visible at day 5 when cells were cultured on TCP than on BSA-MA hydrogels (Figure 7C). Moreover, at day 5, cells cultured on BSA-MA coated substrates still maintained their polygonal shape, while the contours of cells cultured on tissue culture plates were less obvious, probably due to the lack of available space. These results were consistent with previous observations.[12,69] It has been reported that the stiffness of the culture substrates influences the phenotype of hepatocarcinoma cells, with cells maintaining a more differentiated phenotype (e.g., higher albumin synthesis) on soft substrates and cells presenting a more proliferative phenotype when cultured on stiffer 2D substrates.[66] As the formazan dye generated during the CCK-8 reaction is proportional to cell dehydrogenases activity, the relatively higher values observed for cells cultured onto 2D BSA-MA gels, compared to cells cultured on TCP, might be resulting from a relatively increased cell proliferation rate as well as an enhanced metabolic activity.

The adhesion of Huh-7.5 cells onto the 2D BSA gels most probably resulted from the immobilization of adhesive proteins (e.g., laminin, vitronectin) present in the FBS added to the culture media, as reported by other studies with different cell types.[32]

On the basis of these results, we then explored the potential of BSA-MA hydrogels for regenerative medicine applications by encapsulating Huh-7.5 cells within three-dimensional BSA-MA hydrogels (Figure 8). BSA-MA (BSA-MA 3, DM ≈ 100%) hydrogels with different concentrations (10%, 15%, and 20% w/v) were employed to fabricate the cell-laden hydrogels, as BSA-MA 3 gels showed to possess an ample range of physical properties that might differently influence cell behavior. Cells encapsulated in PEGDA hydrogels were used as a control group, as PEGDA hydrogels are known to be relatively inert.[5] Huh-7.5 cells were loaded within BSA-MA 3 and PEGDA hydrogels with a high degree of cell encapsulation efficiency (93.6%, 96.8%, and 93.6% for BSA-MA 3 10%, 15%, and 20% w/v, respectively; 95.5%, 92.3%, and 97.3% for PEGDA 10%, 15%, and 20% w/v, respectively), and no statistical differences were observed among the groups. Viability of the encapsulated cells (Figure 9A) increased in all the hydrogels within the first 4 days, but from day 4 to day 7, it remained stable or increased slightly in the BSA-MA hydrogels, while it decreased in all the PEGDA hydrogels. A calibration curve of the cell number against absorbance readings is provided in Figure S4. Live/Dead fluorescent images of the encapsulated cells at day 1, 4, and 7 supported the CCK-8 results, showing an increase in the number of live cells (green) over time in all the BSA-MA hydrogels and displaying increased dead cells at day 7 in PEGDA hydrogels (Figure 9C). Additionally, independently of the encapsulating scaffolds, Huh-7.5 formed spheroids growing over time, as also observed from the SEM images (Figure 9D). Some dead cells (red) were visible in all the constructs at day 1, indicating that the photo-cross-linking conditions used might have been slightly cytotoxic (Figure 9C), as both UV light and free radicals generated during the photopolymerization process are known to be potentially harmful to cells and tissues.[7] After 7 days in culture, instead, more dead cells were observed in the PEGDA hydrogels, whereas fewer dead cells were found in the BSA-MA hydrogels. SEM images (Figure 9D) also show that Huh-7.5 cells were distributed throughout the entire scaffolds and that they appeared as a round cell or spheroids across all the hydrogel scaffolds, supporting the results of microscopy images.

To evaluate the liver-specific functionality of encapsulated Huh-7.5 cells, albumin secretion in the culture media during a

https://dx.doi.org/10.1021/acsabm.9b00984
ACS Appl. Bio Mater. 2020, 3, 920−934

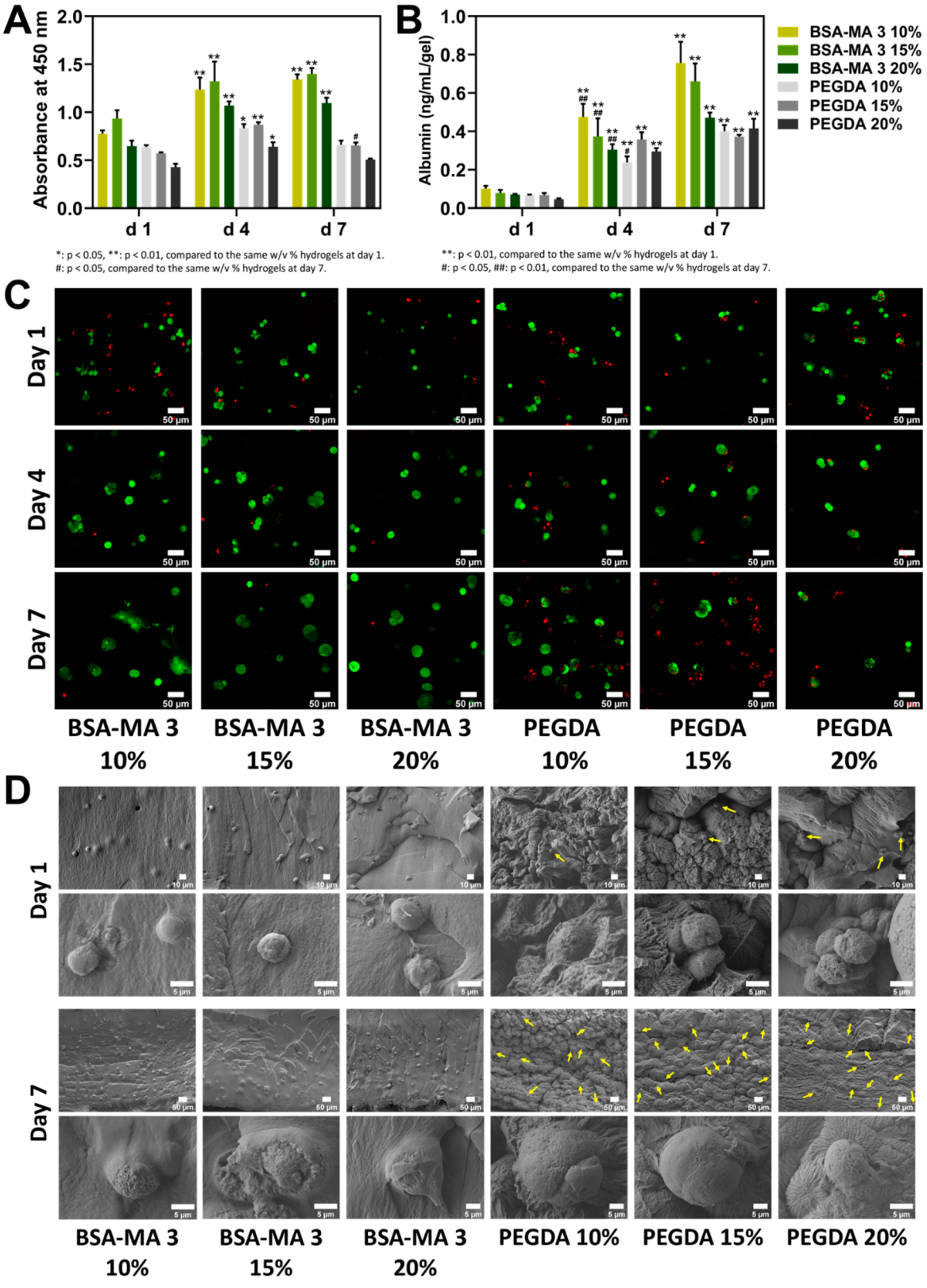

Figure 9. Culture of Huh-7.5 cells encapsulated within BSA-MA 3 and PEGDA hydrogels (10%, 15%, and 20% w/v). (A) Cell viability, as determined by CCK-8 assay. Results are reported as mean ± SD (n = 3). (B) Albumin production within a 24 h period at day 1, 4, and 7. Results are reported as mean ± SD (n = 3). (C) Live/dead staining of encapsulated cells. Fluorescent images were acquired using a confocal microscope with a 20× lens. Live cells were stained green using calcein-AM, and dead cells were stained red using EthD-1. Scale bar is 50 μm. (D) SEM images of the cross-section of cell-laden hydrogels at day 1 and day 7. Yellow arrows point to the encapsulated cells in the PEGDA hydrogels. Scale bars of the images from top to bottom are 10 μm, 5 μm, 50 μm, and 5 μm, respectively.

https://dx.doi.org/10.1021/acsabm.9b00984
ACS Appl. Bio Mater. 2020, 3, 920−934

24 h period was measured. Albumin production increased over time for all the constructs, with the highest increase observed from day 1 to day 4 in all the hydrogels; the increase in albumin production from day 4 to day 7 was more pronounced only in the BSA-MA hydrogels (Figure 9B). Among the BSA-MA hydrogels, those fabricated using lower protein concentrations (10% and 15% w/v) showed higher proliferation rates and albumin secretion, compared to those fabricated with the highest protein content (20% w/v), most probably owing to facile transportation of oxygen and nutrients in hydrogels prepared at a low concentration. These results are consistent with what was previously reported by other studies investigating the effect of various cross-linking densities on cell viability.[61,66,70] Considering the cell viability data (Figure 9A,C), the increase in albumin synthesis over time might be due to both an increase in the cell number and an enhanced cell functionality, though the latter might be the dominant factor from day 4 to day 7, as cells aggregated and formed spheroids. Though both BSA and PEGDA might not interact directly with cells, as indicated by the formation of spheroids in both constructs, BSA-MA hydrogels, due to the innate ability of BSA to bind ECM proteins and other endogenous molecules, might promote cell−cell interactions as well as cell−matrix interactions and thus provide encapsulated cells with a more favorable microenvironment for supporting their proliferation and functionality.

CONCLUSIONS

Here, we systematically investigated, for the first time, the synthesis and properties of photocurable bovine serum albumin methacryloyl hydrogels for tissue engineering applications. BSA-MA with different degrees of methacryloylation was synthesized in a precise manner by controlling the parameters of the reaction and the feed molar ratio of MAA to lysine groups. Methacryloyl functionalization of BSA led to a slight reduction of the BSA α-helical structures, without considerably altering the native structural conformation of BSA molecules. Swelling, mechanical properties, and degradation of photo-cross-linked BSA-MA hydrogels could be easily tuned by changing the degree of functionalization and the macromer concentration, which could offer researchers photocurable protein-based hydrogels with a wide range of properties that can be required for various biomedical applications. Further, BSA-MA hydrogels were cytocompatible and able to support the adhesion and growth of hepatocarcinoma cells. Taken together, this study may pave the way to use photocurable albumin methacryloyl in regenerative medicine applications.

ASSOCIATED CONTENT

Supporting Information

The Supporting Information is available free of charge at https://pubs.acs.org/doi/10.1021/acsabm.9b00984.

Evaluation of degree of methacryloylation of BSA using TNBS assay; ^{1}H NMR spectra of PEGDA; stress−strain curves of BSA-MA hydrogels; calibration curve for CCK-8 assay measurements of 3D cultures (PDF)

AUTHOR INFORMATION

Corresponding Authors

Bae Hoon Lee − *Wenzhou Medical University, Wenzhou, China, and University of CAS, Wenzhou, China;* orcid.org/0000-0002-7222-0008; Email: bhlee@wibe.ac.cn

Nam-Joon Cho − *Nanyang Technological University, Singapore;* orcid.org/0000-0002-8692-8955; Email: njcho@ntu.edu.sg

Other Authors

Gaia Ferracci − *Nanyang Technological University, Singapore*

Mengxiang Zhu − *Wenzhou Medical University, Wenzhou, China, and University of CAS, Wenzhou, China*

Mohammed Shahrudin Ibrahim − *Nanyang Technological University, Singapore*

Gamaliel Ma − *Nanyang Technological University, Singapore*

Teng Fei Fan − *Nanyang Technological University, Singapore*

Complete contact information is available at: https://pubs.acs.org/10.1021/acsabm.9b00984

Notes

The authors declare no competing financial interest.

ACKNOWLEDGMENTS

The authors wish to acknowledge the support from the National Research Foundation (NRF) Singapore Competitive Research Programme (NRF-CRP10-2012-070), the Nanyang Technological University (NTU) - Interdisciplinary Graduate School (IGS), the Zhejiang Provincial Natural Science Foundation of China (Grant No. LGF19E030001), the Wenzhou Medical University (QTJ17012), and the Wenzhou Institute of Biomaterial and Engineering University of CAS (WIUCASQD2019003). The authors wish to thank Yun Yang for assistance with the drawings.

REFERENCES

(1) Singh, T. R. R.; Laverty, G.; Donnelly, R. *Hydrogels: Design, Synthesis and Application in Drug Delivery and Regenerative Medicine*; CRC Press, 2018.

(2) Li, J.; Mooney, D. J. Designing hydrogels for controlled drug delivery. *Nature Reviews Materials* **2016**, *1* (12), 16071.

(3) Caló, E.; Khutoryanskiy, V. V. Biomedical applications of hydrogels: A review of patents and commercial products. *Eur. Polym. J.* **2015**, *65*, 252−267.

(4) Thiele, J.; Ma, Y.; Bruekers, S. M.; Ma, S.; Huck, W. T. 25th anniversary article: designer hydrogels for cell cultures: a materials selection guide. *Adv. Mater.* **2014**, *26* (1), 125−148.

(5) Caliari, S. R.; Burdick, J. A. A practical guide to hydrogels for cell culture. *Nat. Methods* **2016**, *13* (5), 405.

(6) Kim, B.-S.; Mooney, D. J. Development of biocompatible synthetic extracellular matrices for tissue engineering. *Trends Biotechnol.* **1998**, *16* (5), 224−230.

(7) Shirahama, H.; Lee, B. H. Preparation of Photocurable Hydrogels. In *Hydrogels*; CRC Press, 2018; pp 265−283.

(8) Ruedinger, F.; Lavrentieva, A.; Blume, C.; Pepelanova, I.; Scheper, T. Hydrogels for 3D mammalian cell culture: a starting guide for laboratory practice. *Appl. Microbiol. Biotechnol.* **2015**, *99* (2), 623−636.

(9) Brinkman, W. T.; Nagapudi, K.; Thomas, B. S.; Chaikof, E. L. Photo-cross-linking of type I collagen gels in the presence of smooth muscle cells: mechanical properties, cell viability, and function. *Biomacromolecules* **2003**, *4* (4), 890−895.

(10) Yue, K.; Trujillo-de Santiago, G.; Alvarez, M. M.; Tamayol, A.; Annabi, N.; Khademhosseini, A. Synthesis, properties, and biomedical applications of gelatin methacryloyl (GelMA) hydrogels. *Biomaterials* **2015**, *73*, 254−271.
(11) Klotz, B. J.; Gawlitta, D.; Rosenberg, A. J.; Malda, J.; Melchels, F. P. Gelatin-methacryloyl hydrogels: towards biofabrication-based tissue repair. *Trends Biotechnol.* **2016**, *34* (5), 394−407.
(12) Lee, B. H.; Shirahama, H.; Kim, M. H.; Lee, J. H.; Cho, N.-J.; Tan, L. P. Colloidal templating of highly ordered gelatin methacryloyl-based hydrogel platforms for three-dimensional tissue analogues. *NPG Asia Mater.* **2017**, *9* (7), No. e412.
(13) Levett, P. A.; Melchels, F. P.; Schrobback, K.; Hutmacher, D. W.; Malda, J.; Klein, T. J. A biomimetic extracellular matrix for cartilage tissue engineering centered on photocurable gelatin, hyaluronic acid and chondroitin sulfate. *Acta Biomater.* **2014**, *10* (1), 214−223.
(14) Nettles, D. L.; Vail, T. P.; Morgan, M. T.; Grinstaff, M. W.; Setton, L. A. Photocrosslinkable hyaluronan as a scaffold for articular cartilage repair. *Ann. Biomed. Eng.* **2004**, *32* (3), 391−397.
(15) Gao, S.; Zhao, P.; Lin, C.; Sun, Y.; Wang, Y.; Zhou, Z.; Yang, D.; Wang, X.; Xu, H.; Zhou, F.; et al. Differentiation of human adipose-derived stem cells into neuron-like cells which are compatible with photocurable three-dimensional scaffolds. *Tissue Eng., Part A* **2014**, *20* (7−8), 1271−1284.
(16) Chou, A. I.; Akintoye, S. O.; Nicoll, S. B. Photo-crosslinked alginate hydrogels support enhanced matrix accumulation by nucleus pulposus cells in vivo. *Osteoarthritis and cartilage* **2009**, *17* (10), 1377−1384.
(17) Liu, Y.; Chan-Park, M. B. A biomimetic hydrogel based on methacrylated dextran-graft-lysine and gelatin for 3D smooth muscle cell culture. *Biomaterials* **2010**, *31* (6), 1158−1170.
(18) Corrente, F.; Amara, H. M. A.; Pacelli, S.; Paolicelli, P.; Casadei, M. A. Novel injectable and in situ cross-linkable hydrogels of dextran methacrylate and scleroglucan derivatives: Preparation and characterization. *Carbohydr. Polym.* **2013**, *92* (2), 1033−1039.
(19) Bessonov, I. V.; Rochev, Y. A.; Arkhipova, A. Y.; Kopitsyna, M. N.; Bagrov, D. V.; Karpushkin, E. A.; Bibikova, T. N.; Moysenovich, A. M.; Soldatenko, A. S.; Nikishin, I. I.; et al. Fabrication of hydrogel scaffolds via photocrosslinking of methacrylated silk fibroin. *Biomedical Materials* **2019**, *14* (3), 034102.
(20) Annabi, N.; Tsang, K.; Mithieux, S. M.; Nikkhah, M.; Ameri, A.; Khademhosseini, A.; Weiss, A. S. Highly elastic micropatterned hydrogel for engineering functional cardiac tissue. *Adv. Funct. Mater.* **2013**, *23* (39), 4950−4959.
(21) Merlot, A. M.; Kalinowski, D. S.; Richardson, D. R. Unraveling the mysteries of serum albumin - more than just a serum protein. *Front. Physiol.* **2014**, *5*, 299.
(22) Kragh-Hansen, U. Human serum albumin: a multifunctional protein. In *Albumin in Medicine*; Springer, 2016; pp 1−24.
(23) Kratz, F. A clinical update of using albumin as a drug vehicle—A commentary. *J. Controlled Release* **2014**, *190*, 331−336.
(24) Aiyelabegan, H. T.; Zaidi, S. S.; Fanuel, S.; Eatemadi, A.; Ebadi, M. T.; Sadroddiny, E. Albumin-based biomaterial for lung tissue engineering applications. *Int. J. Polym. Mater.* **2016**, *65* (16), 853−861.
(25) Ong, J.; Zhao, J.; Justin, A. W.; Markaki, A. E. Albumin-Based Hydrogels for Regenerative Engineering and Cell Transplantation. *Biotechnol. Bioeng.* **2019**, *116*, 3457−3468.
(26) Lexa, K. W.; Dolghih, E.; Jacobson, M. P. A structure-based model for predicting serum albumin binding. *PLoS One* **2014**, *9* (4), No. e93323.
(27) Baler, K.; Michael, R.; Szleifer, I.; Ameer, G. A. Albumin hydrogels formed by electrostatically triggered self-assembly and their drug delivery capability. *Biomacromolecules* **2014**, *15* (10), 3625−3633.
(28) Li, P.-S.; Lee, I.-L.; Yu, W.-L.; Sun, J.-S.; Jane, W.-N.; Shen, H.-H. A novel albumin-based tissue scaffold for autogenic tissue engineering applications. *Sci. Rep.* **2015**, *4*, 5600.
(29) Hsu, C.-C.; Serio, A.; Amdursky, N.; Besnard, C.; Stevens, M. M. Fabrication of hemin-doped serum albumin-based fibrous scaffolds for neural tissue engineering applications. *ACS Appl. Mater. Interfaces* **2018**, *10* (6), 5305−5317.
(30) Nseir, N.; Regev, O.; Kaully, T.; Blumenthal, J.; Levenberg, S.; Zussman, E. Biodegradable scaffold fabricated of electrospun albumin fibers: mechanical and biological characterization. *Tissue Eng., Part C* **2013**, *19* (4), 257−264.
(31) Amdursky, N.; Mazo, M. M.; Thomas, M. R.; Humphrey, E. J.; Puetzer, J. L.; St-Pierre, J.-P.; Skaalure, S. C.; Richardson, R. M.; Terracciano, C. M.; Stevens, M. M. Elastic serum-albumin based hydrogels: mechanism of formation and application in cardiac tissue engineering. *J. Mater. Chem. B* **2018**, *6* (35), 5604−5612.
(32) Fleischer, S.; Shapira, A.; Regev, O.; Nseir, N.; Zussman, E.; Dvir, T. Albumin fiber scaffolds for engineering functional cardiac tissues. *Biotechnol. Bioeng.* **2014**, *111* (6), 1246−1257.
(33) Iemma, F.; Spizzirri, U.; Muzzalupo, R.; Puoci, F.; Trombino, S.; Picci, N. Spherical hydrophilic microparticles obtained by the radical copolymerisation of functionalised bovine serum albumin. *Colloid Polym. Sci.* **2004**, *283* (3), 250−256.
(34) Iemma, F.; Spizzirri, U.; Puoci, F.; Muzzalupo, R.; Trombino, S.; Picci, N. Radical crosslinked albumin microspheres as potential drug delivery systems: preparation and in vitro studies. *Drug Delivery* **2005**, *12* (3), 179−184.
(35) Iemma, F.; Spizzirri, U. G.; Puoci, F.; Muzzalupo, R.; Trombino, S.; Cassano, R.; Leta, S.; Picci, N. pH-Sensitive hydrogels based on bovine serum albumin for oral drug delivery. *Int. J. Pharm.* **2006**, *312* (1−2), 151−157.
(36) Iemma, F.; Spizzirri, U.; Puoci, F.; Cirillo, G.; Curcio, M.; Parisi, O.; Picci, N. Synthesis and release profile analysis of thermo-sensitive albumin hydrogels. *Colloid Polym. Sci.* **2009**, *287* (7), 779−787.
(37) Abbate, V.; Kong, X.; Bansal, S. S. Photocrosslinked bovine serum albumin hydrogels with partial retention of esterase activity. *Enzyme Microb. Technol.* **2012**, *50* (2), 130−136.
(38) Shirahama, H.; Lee, B. H.; Tan, L. P.; Cho, N. J. Precise Tuning of Facile One-Pot Gelatin Methacryloyl (GelMA) Synthesis. *Sci. Rep.* **2016**, *6*, 31036.
(39) Zhu, M.; Wang, Y.; Ferracci, G.; Zheng, J.; Cho, N.-J.; Lee, B. H. Gelatin methacryloyl and its hydrogels with an exceptional degree of controllability and batch-to-batch consistency. *Sci. Rep.* **2019**, *9*, 1−13.
(40) Lee, B. H.; Shirahama, H.; Cho, N.-J.; Tan, L. P. Efficient and controllable synthesis of highly substituted gelatin methacrylamide for mechanically stiff hydrogels. *RSC Adv.* **2015**, *5* (128), 106094−106097.
(41) Claaßen, C.; Claaßen, M. H.; Truffault, V.; Sewald, L.; Tovar, G. n. E.; Borchers, K.; Southan, A. Quantification of substitution of gelatin methacryloyl: best practice and current pitfalls. *Biomacromolecules* **2018**, *19* (1), 42−52.
(42) Greenfield, N. J. Using circular dichroism spectra to estimate protein secondary structure. *Nat. Protoc.* **2006**, *1* (6), 2876.
(43) Kelly, S. M.; Jess, T. J.; Price, N. C. How to study proteins by circular dichroism. *Biochim. Biophys. Acta, Proteins Proteomics* **2005**, *1751* (2), 119−139.
(44) Corrêa, D. H.; Ramos, C. H. The use of circular dichroism spectroscopy to study protein folding, form and function. *African Journal of Biochemistry Research* **2009**, *3* (5), 164−173.
(45) Yang, H.; Yang, S.; Kong, J.; Dong, A.; Yu, S. Obtaining information about protein secondary structures in aqueous solution using Fourier transform IR spectroscopy. *Nat. Protoc.* **2015**, *10* (3), 382.
(46) Murayama, K.; Tomida, M. Heat-induced secondary structure and conformation change of bovine serum albumin investigated by Fourier transform infrared spectroscopy. *Biochemistry* **2004**, *43* (36), 11526−11532.
(47) Barth, A. Infrared spectroscopy of proteins. *Biochim. Biophys. Acta, Bioenerg.* **2007**, *1767* (9), 1073−1101.

https://dx.doi.org/10.1021/acsabm.9b00984
ACS Appl. Bio Mater. 2020, 3, 920−934

(48) Srour, B.; Bruechert, S.; Andrade, S. L.; Hellwig, P. Secondary Structure Determination by Means of ATR-FTIR Spectroscopy. In *Membrane Protein Structure and Function Characterization*; Springer, 2017; pp 195−203.
(49) Kim, M. H.; Kumar, S. K.; Shirahama, H.; Seo, J.; Lee, J. H.; Zhdanov, V. P.; Cho, N. J. Biofunctionalized hydrogel microscaffolds promote 3D hepatic sheet morphology. *Macromol. Biosci.* **2016**, *16* (3), 314−321.
(50) Peters, Jr., T. *All about Albumin: Biochemistry, Genetics, and Medical Applications*; Academic Press, 1995.
(51) Yue, K.; Li, X.; Schrobback, K.; Sheikhi, A.; Annabi, N.; Leijten, J.; Zhang, W.; Zhang, Y. S.; Hutmacher, D. W.; Klein, T. J.; et al. Structural analysis of photocrosslinkable methacryloyl-modified protein derivatives. *Biomaterials* **2017**, *139*, 163−171.
(52) Zheng, J.; Zhu, M.; Ferracci, G.; Cho, N. J.; Lee, B. H. Hydrolytic Stability of Methacrylamide and Methacrylate in Gelatin Methacryloyl and Decoupling of Gelatin Methacrylamide from Gelatin Methacryloyl through Hydrolysis. *Macromol. Chem. Phys.* **2018**, *219* (18), 1800266.
(53) Hoch, E.; Schuh, C.; Hirth, T.; Tovar, G. E.; Borchers, K. Stiff gelatin hydrogels can be photo-chemically synthesized from low viscous gelatin solutions using molecularly functionalized gelatin with a high degree of methacrylation. *J. Mater. Sci.: Mater. Med.* **2012**, *23* (11), 2607−2617.
(54) *UniProtKB P02769*; UniProt Consortium, 2020. https://www.uniprot.org/.
(55) Oakes, J. Protein hydration. Nuclear magnetic resonance relaxation studies of the state of water in native bovine serum albumin solutions. *J. Chem. Soc., Faraday Trans. 1* **1976**, *72*, 216−227.
(56) Lindblad, W. J.; Diegelmann, R. F. Quantitation of hydroxyproline isomers in acid hydrolysates by high-performance liquid chromatography. *Anal. Biochem.* **1984**, *138* (2), 390−395.
(57) Martinez-Saez, N.; Fernandez-Gomez, B.; Cai, W.; Uribarri, J.; Del Castillo, M. D. In vitro formation of Maillard reaction products during simulated digestion of meal-resembling systems. *Food Res. Int.* **2019**, *118*, 72−80.
(58) Bujacz, A. Structures of bovine, equine and leporine serum albumin. *Acta Crystallogr., Sect. D: Biol. Crystallogr.* **2012**, *68* (10), 1278−1289.
(59) Hoch, E.; Hirth, T.; Tovar, G. E.; Borchers, K. Chemical tailoring of gelatin to adjust its chemical and physical properties for functional bioprinting. *J. Mater. Chem. B* **2013**, *1* (41), 5675−5685.
(60) Kim, S. H.; Chu, C. C. Synthesis and characterization of dextran-methacrylate hydrogels and structural study by SEM. *J. Biomed. Mater. Res.* **2000**, *49* (4), 517−527.
(61) Burdick, J. A.; Chung, C.; Jia, X.; Randolph, M. A.; Langer, R. Controlled degradation and mechanical behavior of photopolymerized hyaluronic acid networks. *Biomacromolecules* **2005**, *6* (1), 386−391.
(62) Zhao, X.; Lang, Q.; Yildirimer, L.; Lin, Z. Y.; Cui, W.; Annabi, N.; Ng, K. W.; Dokmeci, M. R.; Ghaemmaghami, A. M.; Khademhosseini, A. Photocrosslinkable gelatin hydrogel for epidermal tissue engineering. *Adv. Healthcare Mater.* **2016**, *5* (1), 108−118.
(63) Annabi, N.; Mithieux, S. M.; Zorlutuna, P.; Camci-Unal, G.; Weiss, A. S.; Khademhosseini, A. Engineered cell-laden human protein-based elastomer. *Biomaterials* **2013**, *34* (22), 5496−5505.
(64) Engler, A. J.; Sen, S.; Sweeney, H. L.; Discher, D. E. Matrix elasticity directs stem cell lineage specification. *Cell* **2006**, *126* (4), 677−689.
(65) Jabbari, E.; Sarvestani, S. K.; Daneshian, L.; Moeinzadeh, S. Optimum 3D matrix stiffness for maintenance of cancer stem cells is dependent on tissue origin of cancer cells. *PLoS One* **2015**, *10* (7), No. e0132377.
(66) Schrader, J.; Gordon-Walker, T. T.; Aucott, R. L.; van Deemter, M.; Quaas, A.; Walsh, S.; Benten, D.; Forbes, S. J.; Wells, R. G.; Iredale, J. P. Matrix stiffness modulates proliferation, chemotherapeutic response, and dormancy in hepatocellular carcinoma cells. *Hepatology* **2011**, *53* (4), 1192−1205.
(67) Seliktar, D. Designing cell-compatible hydrogels for biomedical applications. *Science* **2012**, *336* (6085), 1124−1128.
(68) Agudelo, D.; Bourassa, P.; Bruneau, J.; Berube, G.; Asselin, É.; Tajmir-Riahi, H.-A. Probing the binding sites of antibiotic drugs doxorubicin and N-(trifluoroacetyl) doxorubicin with human and bovine serum albumins. *PLoS One* **2012**, *7* (8), No. e43814.
(69) Sainz, B., Jr; Barretto, N.; Uprichard, S. L. Hepatitis C virus infection in phenotypically distinct Huh7 cell lines. *PLoS One* **2009**, *4* (8), No. e6561.
(70) Lee, B. H.; Kim, M. H.; Lee, J. H.; Seliktar, D.; Cho, N. J.; Tan, L. P. Modulation of Huh7.5 spheroid formation and functionality using modified PEG-based hydrogels of different stiffness. *PLoS One* **2015**, *10* (2), No. e0118123.

https://dx.doi.org/10.1021/acsabm.9b00984
ACS Appl. Bio Mater. 2020, 3, 920−934